Effects of nonlinear energy transfer on short surface waves

David R. Lyzenga[1]

Received 2 October 2009; revised 6 May 2010; accepted 9 June 2010; published 2 October 2010.

[1] The effects of nonlinear energy transfer on the development of the short wave spectrum are evaluated using a diffusion approximation and a modification of this approximation to include nonlocal effects. Both formulations were used to compute the evolution of a JONSWAP-type spectrum, and the results are compared with direct numerical simulations. Terms corresponding to each of these formulations were then incorporated into the wave action equation, and the resulting equation was numerically integrated using a second-order Runge-Kutta method. The results show an increase in the angular width of the spectrum and in the spectral density at high wave numbers as compared with solutions of the action equation without the nonlinear energy transfer term. Example results are presented for the case of a moderately strong internal wave in a light wind, and implications for the remote sensing of these waves using microwave radar are discussed.

Citation: Lyzenga, D. R. (2010), Effects of nonlinear energy transfer on short surface waves, *J. Geophys. Res.*, *115*, C10001, doi:10.1029/2009JC005872.

1. Introduction

[2] Modeling of the microwave radar signatures of oceanic internal wave and current fronts has traditionally been done using the wave action equation, coupled with a Bragg or two-scale radar backscatter model [e.g., *Lyzenga and Bennett*, 1988; *Thompson et al.*, 1988; *Thompson*, 1988]. The wave action equation describes the changes in the amplitude or spectral density of surface waves due to their interactions with spatially variable surface currents. This equation also includes the generation and growth of waves by the wind, dissipation by molecular viscosity and nonlinear effects, and in principle energy transfer among waves of different wavelengths due to nonlinear interactions, although the latter have largely been neglected in the past because of the complexity and computational cost of including them. Most of the interest in this context is in wavelengths on the order of centimeters, because of their influence on the backscatter of electromagnetic waves in the microwave region, which are most useful for remote sensing purposes. However, longer-scale waves are also strongly perturbed by internal waves and current fronts. Thus, the coupling of these longer waves with centimeter-scale waves cannot safely be neglected.

[3] In this paper, the roles and effects of nonlinear surface wave interactions are investigated using the diffusion approximation of *Jenkins and Phillips* [2001] as well as a simple modification of this approximation. The evolution of a JONSWAP-type spectrum is computed using these approximations, and the results are compared with direct numerical simulations reported by *Tanaka* [2001, 2007] and *Yokoyama* [2004]. Terms corresponding to these approximations are then incorporated into the wave action equation, numerical solutions of the wave action equation with the added terms are described, and solutions with and without the nonlinear transfer terms are compared and discussed.

2. Wave Action Equation

[4] The wave action equation can be written in fixed wave number coordinates [*Phillips*, 1984; *Lyzenga and Bennett*, 1988] as

$$\frac{\partial N}{\partial t} + (c_{gx} + u)\frac{\partial N}{\partial x} + (c_{gy} + v)\frac{\partial N}{\partial y} - \left(k_x \frac{\partial u}{\partial x} + k_y \frac{\partial v}{\partial x}\right)\frac{\partial N}{\partial k_x} - \left(k_x \frac{\partial u}{\partial y} + k_y \frac{\partial v}{\partial y}\right)\frac{\partial N}{\partial k_y} = F_s(N), \quad (1)$$

where $N(k_x, k_y, x, y, t)$ is the action spectral density, $\boldsymbol{k} = (k_x, k_y)$ is the wave number vector, $\boldsymbol{c}_g = (c_{gx}, c_{gy})$ is the group velocity, and $\boldsymbol{u} = (u,v)$ is the surface current. The quantity $F_s(N)$ on the right-hand side of the equation is the net source function, which accounts for wind input, wave energy dissipation, and nonlinear wave-wave interactions. Using polar coordinates with ϕ being the wave propagation direction measured clockwise from the x axis and $\kappa = \ln(k)$, the wave action equation becomes

$$\frac{\partial N}{\partial t} + V_x \frac{\partial N}{\partial x} + V_y \frac{\partial N}{\partial y} + V_\kappa \frac{\partial N}{\partial \kappa} + V_\phi \frac{\partial N}{\partial \phi} = F_s(N), \quad (2)$$

where $V_x = c_{gx} + u$, $V_y = c_{gy} + v$, $V_\kappa = -\cos^2\phi \frac{\partial u}{\partial x} + \cos\phi \sin\phi \left(\frac{\partial v}{\partial x} + \frac{\partial u}{\partial y}\right) - \sin^2\phi \frac{\partial v}{\partial y}$, and $V_\phi = -\sin^2\phi \frac{\partial v}{\partial x} + \cos\phi \sin\phi \left(\frac{\partial u}{\partial x} - \frac{\partial v}{\partial y}\right) + \cos^2\phi \frac{\partial u}{\partial y}$. Equation (2) can also be written in terms of the linear wave number k, the frequency ω, or the

[1]Naval Architecture and Marine Engineering Department, University of Michigan, Ann Arbor, Michigan, USA.

0148-0227/10/2009JC005872

logarithmic frequency $w = \ln(\omega)$ by replacing V_κ with $V_k = kV_\kappa$, $V_\omega = c_g V_k$, or $V_w = (c_g/c)V_\kappa$, respectively. Using $N = \rho c B k^{-4}$, where $B = k^4 S(k, \phi)$ is the dimensionless saturation or curvature spectrum, this equation can also be written as

$$\frac{\partial B}{\partial t} + V_x \frac{\partial B}{\partial x} + V_y \frac{\partial B}{\partial y} + V_\kappa \frac{\partial B}{\partial \kappa} + V_\phi \frac{\partial B}{\partial \phi} = F_s(B) + V_\kappa (5 - \frac{c_g}{c})\, B. \tag{3}$$

If the x axis is oriented at an angle ϕ_x measured clockwise from north, the wave propagation direction relative to north is $\phi + \phi_x$ and the wave propagation direction relative to the wind direction ϕ_w (also measured clockwise from north) is $\phi_r = \phi + \phi_x - \phi_w$.

3. Source Function

[5] Using a wind input term that is proportional to the spectral density [*Snyder et al.*, 1981; *Plant*, 1982] and a dissipation term proportional to the cube of the spectral density [*Phillips*, 1985], the source function for the curvature spectrum $B(k, \phi)$ can be written as

$$F_s(B) = (\beta - 4\nu k^2)B - \alpha_0 \omega B^3 + F_{nl}(B), \tag{4}$$

where β is the wind growth rate, ν is the kinematic viscosity of water, and $F_{nl}(B)$ is the source term due to nonlinear wave-wave interactions. A theory for nonlinear resonant interactions among gravity waves has been developed by *Hasselmann* [1962] and others, but this theory requires the evaluation of a sixfold integral in wave number space, which is not practical for inclusion in wave-current interaction models of the type described later in this section. The effects of nonlinear interactions can also be seen in direct numerical simulations of surface gravity wave evolution, such as those by *Tanaka* [2001, 2007] and *Yokoyama* [2004]. However, such simulations are also impractical for routine application to the remote sensing problems discussed below. *Jenkins and Phillips* [2001] showed that a nonlinear source term of the form

$$F_{nl}(B) = \alpha_1 \left(\frac{\partial \omega}{\partial k}\right) \left[\frac{\partial^2 \psi}{\partial \omega^2} + \frac{1}{k}\left(\frac{\partial^2 k}{\partial \omega^2}\right)\frac{\partial^2 \psi}{\partial \phi^2}\right] \omega k^3 \tag{5}$$

conserves energy, action, and momentum for any function $\psi(\boldsymbol{k})$ that goes to zero rapidly enough as $k \to 0$ and $k \to \infty$. Using the gravity wave dispersion relation and defining

$$\psi = \frac{\omega}{k^2} B^3(k, \phi) \tag{6}$$

as proposed by *Jenkins and Phillips* [2001] on dimensional grounds, this formulation for the nonlinear energy transfer term is equivalent to the diffusion approximation of *Polnikov* [2002] and *Polnikov et al.* [2002]. Equation (5) is also valid when surface tension effects are included, in which case it can be written as

$$F_{nl}(B) = \alpha_1 k^3 \left[c_g \omega \frac{\partial^2 \psi}{\partial \omega^2} + \frac{1}{k}\left(1 - \frac{3\tau k}{c_g^2}\right)\frac{\partial^2 \psi}{\partial \phi^2}\right], \tag{7}$$

where τ is the ratio of the surface tension to the density of water. The term involving $\partial^2\psi/\partial\phi^2$ in (7) causes an increase in the angular width of the spectrum at intermediate wavelengths, but the factor $1 - 3\tau k/c_g^2$ causes the spectrum to narrow again at high wave numbers. This behavior is consistent with the properties of the wave spectra inferred from microwave scatterometry data (see Figure 10 and the related discussion in section 5 below).

[6] The inclusion of surface tension effects calls into question the appropriateness of the form of the ψ function in (6), however. The dependence on the cube of the spectral density in (6) is consistent with the fact that resonant interactions among gravity waves occur at third order, i.e., among sets of four wave numbers. Resonant interactions occur among gravity-capillary waves at both second and third orders, i.e., among sets of three as well as four wave components, so the source function for such interactions may be expected to have terms proportional to the square as well as the cube of the spectral density. However, there is little information at present on the relative magnitudes of these terms, and in the absence of such information we have chosen to neglect second-order terms for the present. The scale factors for the cubic terms are determined by comparisons with the Hasselmann theory for gravity waves (see Figure 1), and surface tension effects have been omitted for the purpose of these comparisons as well as for comparison with Tanaka's and Yokoyama's gravity wave simulations (Figures 2–7).

[7] Surface tension effects have been included in the calculations described in section 5, however, because these effects are known to be important in the wave number region of interest for microwave radar backscatter calculations. This inclusion is not necessarily inconsistent with the neglect of second-order terms, since gravity-capillary waves interact at both second and third orders, but this neglect means that our results are probably incomplete and may be considered as providing a lower bound for nonlinear interaction effects involving gravity-capillary waves at high wave numbers. The second-order terms must go to zero for gravity waves, and presumably transition smoothly (i.e., increase slowly) as the wave number increases into the region where capillary effects are important, so the results presented here should be valid for at least the lower part of the gravity-capillary regime.

[8] The source function (7) can be written in terms of the logarithmic frequency w as

$$F_{nl}(B) = \alpha_1 k^2 \left[\frac{c_g}{c}\left(\frac{\partial^2 \psi}{\partial w^2} - \frac{\partial \psi}{\partial w}\right) + \left(1 - \frac{3\tau k}{c_g^2}\right)\frac{\partial^2 \psi}{\partial \phi^2}\right]. \tag{8}$$

The first derivative in this equation can be eliminated by defining $y = \omega^{-1/2}\psi$, which results in the expression

$$F_{nl}(B) = \alpha_1 k^2 \omega^{1/2} \left[\frac{c_g}{c}\left(\frac{\partial^2 y}{\partial w^2} - \frac{y}{4}\right) + \left(1 - \frac{3\tau k}{c_g^2}\right)\frac{\partial^2 y}{\partial \phi^2}\right]. \tag{9}$$

Using equation (6), the term involving $y/4$ becomes $\frac{1}{4}\alpha_1 (c_g/c) B^3$. An evolution equation for B in the absence of currents can then be written as

$$\frac{\partial B}{\partial t} = (\beta - 4\nu k^2)B - \alpha_0' \omega B^3 + \alpha_1 k^2 \omega^{1/2} \left[\left(\frac{c_g}{c}\right)\frac{\partial^2 y}{\partial w^2} + \left(1 - \frac{3\tau k}{c_g^2}\right)\frac{\partial^2 y}{\partial \phi^2}\right], \tag{10}$$

where $\alpha_0' = \alpha_0 + \frac{1}{4}\alpha_1 c_g/c$.

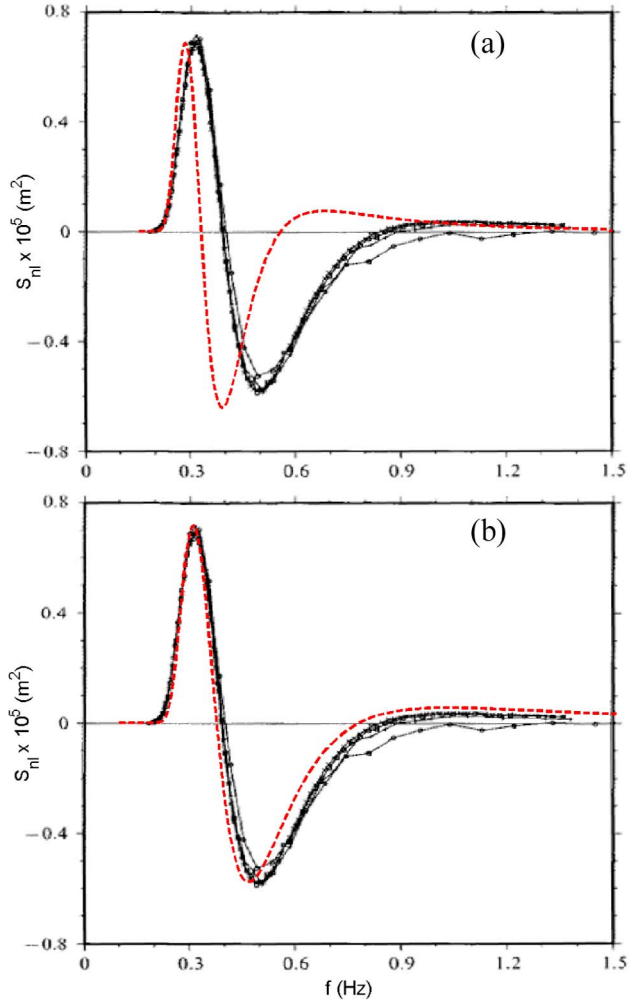

Figure 1. Comparison of nonlinear source terms from *Resio and Perrie* [1991] (solid lines) with approximate source terms (dashed lines) using (a) the diffusion approximation of Jenkins and Phillips with $\alpha_1 = 2.5$ and (b) the modified version of this approximation with $\alpha_1 = 20$.

[9] The diffusion approximation discussed above accounts only for local interactions in wave number space, since it only involves derivatives of the spectrum, but the resonant interaction theory also involves nonlocal interactions among widely spaced wave numbers. Such nonlocal interactions can be incorporated heuristically by redefining the function $\psi(\boldsymbol{k})$ as

$$\psi = \frac{\omega}{k^2}\int_0^w B^3(w',\phi)\,\mathrm{d}w', \tag{11}$$

which still satisfies the requirements stated by *Jenkins and Phillips* [2001]. The derivative of this function with respect to w can be written as

$$\frac{\partial\psi}{\partial w} = \frac{\omega}{k^2}B^3 + \left(1 - 2c/c_g\right)\psi\,. \tag{12}$$

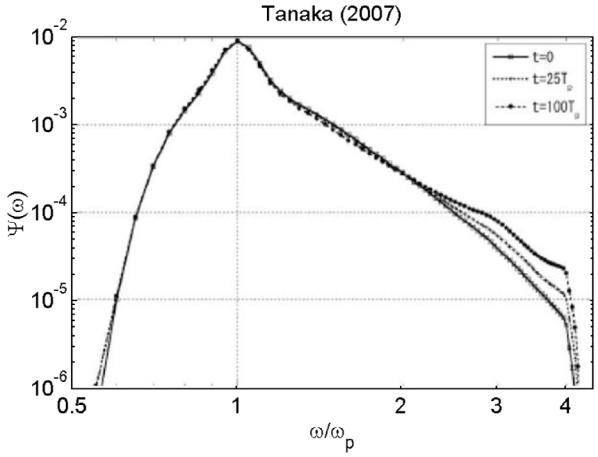

Figure 2. Evolution of normalized frequency spectra from numerical simulations by *Tanaka* [2007].

Thus, it is not necessary to make an additional change of variable to eliminate the first derivative in equation (8). The nonlinear source function then becomes

$$F_{nl}(B) = \alpha_1 k^2\left[\frac{c_g}{c}\left(\frac{\partial^2\psi}{\partial w^2}\right) + \left(1 - \frac{3\tau k}{c_g^2}\right)\frac{\partial^2\psi}{\partial\phi^2} + \left(2 - \frac{c_g}{c}\right)\psi - \frac{c_g}{k}B^3\right]. \tag{13}$$

Using this formulation, the evolution equation for B in the absence of currents is

$$\frac{\partial B}{\partial t} = \left(\beta - 4\nu k^2\right)B - \alpha_0'\,\omega B^3 + \alpha_1 k^2\left(2 - \frac{c_g}{c}\right)\psi + \alpha_1 k^2\left[\left(\frac{c_g}{c}\right)\frac{\partial^2\psi}{\partial w^2} + \left(1 - \frac{3\tau k}{c_g^2}\right)\frac{\partial^2\psi}{\partial\phi^2}\right], \tag{14}$$

where $\alpha_0' = \alpha_0 + \alpha_1 c_g/c$.

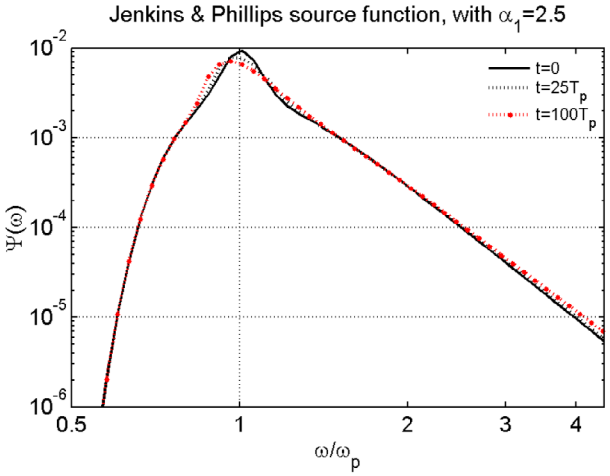

Figure 3. Normalized frequency spectra from growth model using nonlinear source term of *Jenkins and Phillips* [2001] with $\alpha_1 = 2.5$.

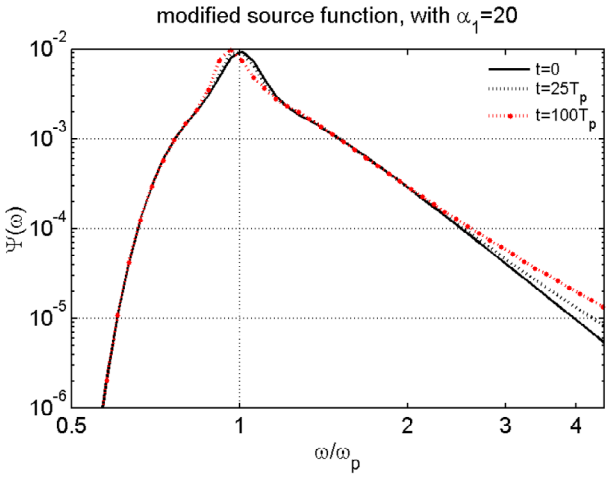

Figure 4. Normalized frequency spectra from growth model using modified version of *Jenkins and Phillips* source term with $\alpha_1 = 20$.

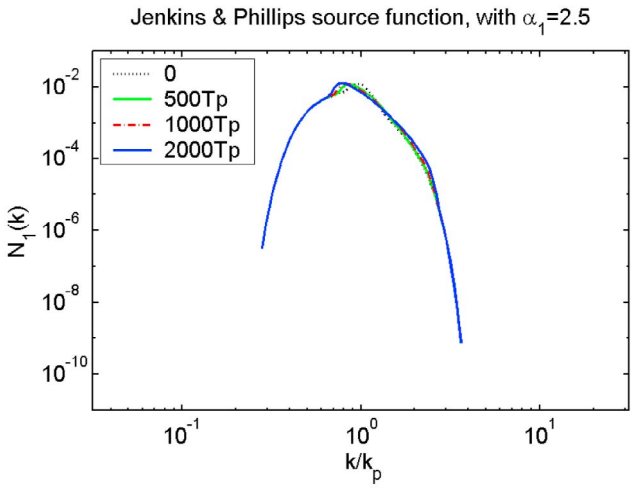

Figure 6. Normalized 1-D action spectra using *Jenkins and Phillips* [2001] source term.

[10] The nonlinear transfer terms for both of these formulations, i.e., using (6) and (11), are compared in Figure 1 with numerical evaluations of Hasselmann's theory by *Resio and Perrie* [1991] for the Pierson-Moskowitz spectrum

$$S(f,\phi) = (2\pi)^{-4}\,\alpha g^2 f^{-5} e^{-1.25\left(f_p/f\right)^4}\,\Phi(\phi-\phi_w), \qquad (15)$$

with $\alpha = 0.01$, $f_p = 0.3$ Hz, and $\Phi(\phi) = (2/\pi)\cos^2\phi$ for $|\phi| < \pi/2$. For purposes of this comparison the source function term for B given in (5) was converted into the equivalent source function for the frequency spectrum, i.e.,

$$S_{nl} = 2\pi k^{-3} c_g^{-1} F_{nl}(B). \qquad (16)$$

A scale factor of $\alpha_1 = 2.5$ was used for the original Jenkins and Phillips formulation (6) and $\alpha_1 = 20$ was used for the modified version (11), to approximately match the magnitude of the source function calculated by *Resio and Perrie* [1991]. Both formulations show qualitatively similar features, but the modified version agrees much more closely with the Hasselmann theory, at least for the Pierson-Moskowitz spectrum.

[11] In order to further test these formulations, the evolution of an initial wave spectrum due to the source functions (9) and (13) was computed and the results were compared with the numerical simulations made by *Tanaka* [2001, 2007] and *Yokoyama* [2004]. In order to match the conditions of these simulations, the growth and dissipation terms in (10) and (14) were omitted (although the artificial dissipation term used by *Yokoyama* was included for the comparisons with his results, see below). The simulations by *Tanaka* [2007] were done using a variant of the JONSWAP spectrum, which can be written as

$$S(\omega,\phi) = \alpha g^2 \omega^{-5} e^{-1.25\left(\omega_p/\omega\right)^4}\,\gamma^{\exp\left[-\frac{1}{2}(\omega/\omega_p-1)^2/\sigma^2\right]}\,G(\phi), \qquad (17)$$

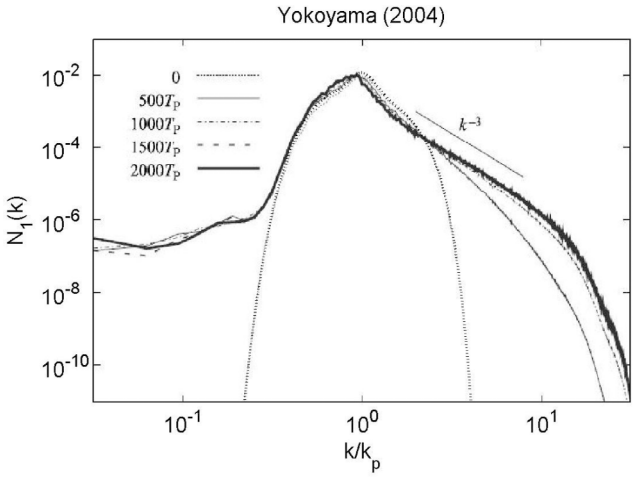

Figure 5. Normalized 1-D action spectra from numerical simulations by *Yokoyama* [2004].

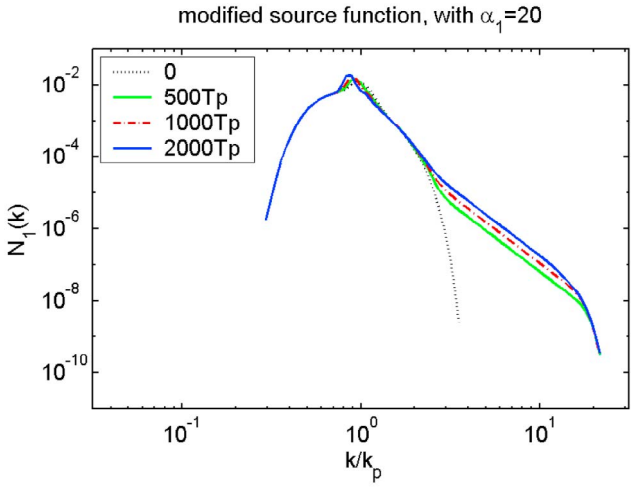

Figure 7. Normalized 1-D action spectra using modified *Jenkins and Phillips* source term.

where $\alpha = \pi E e^{5/4}/\gamma$, $E = \langle \eta^2 \rangle \omega_p^4/g^2$ is the nondimensional energy density, ω_p is the peak frequency, $\gamma = 3.3$, and

$$\sigma = \begin{cases} 0.07 & (\omega < \omega_p) \\ 0.09 & (\omega \geq \omega_p) \end{cases}. \tag{18}$$

Results were presented by *Tanaka* in the form of the nondimensional spectrum

$$\Psi(\omega) = \omega_p^5/g^2 \int_{-\pi}^{\pi} S(\omega, \phi) \mathrm{d}\phi, \tag{19}$$

which was calculated at $t = 0$, $25T_p$ and $100T_p$ (where $T_p = 2\pi/\omega_p$) using an initial spectrum with an angular distribution $G(\phi) = (2/\pi)\cos^2\phi$ (for $|\phi| < \pi/2$) and a nondimensional energy density $E = 0.003$. A plot of these results is reproduced in Figure 2. The corresponding results obtained by integrating (10) and (14) (without the growth and dissipation terms) are shown in Figures 3 and 4, respectively. These equations were integrated using a Runge-Kutta method as described in the following section. The same constants as in Figure 1 ($\alpha_1 = 2.5$ for the original Jenkins and Phillips formulation and $\alpha_1 = 20$ for the modified formulation) were used for this calculation. A peak wave period of 5 s was used for both models, although the normalized results are independent of this value because surface tension effects are not included. Both models show an increase in the spectral density at frequencies above the spectral peak, but the second model produces much larger increases at high frequencies, in closer agreement with Tanaka's results. Both models also show a slight downshift of the spectral peak as expected, although this downshift does not appear in Tanaka's results over the time scales shown.

[12] The results presented by *Yokoyama* [2004] were generated using the same spectral form as *Tanaka* but with an additional factor of $e^{-(k/k_c)^4}$ where $k_c = 2k_p$, which produces a much faster falloff at frequencies above the spectral peak. He also used an isotropic angular distribution and selected a scale factor to produce a normalized energy density of 0.005 (instead of 0.003). In addition, *Yokoyama* included an artificial dissipation proportional to k^{16} in his evolution equation for the spectral amplitude, for numerical stability purposes. *Yokoyama*'s results are presented in the form of the normalized 1-D action spectrum,

$$N_1(k) = \omega_p k_p^3 \int_{-\pi}^{\pi} kN(k, \phi) \mathrm{d}\phi, \tag{20}$$

where $N(k, \phi) = S(k, \phi)/\omega$ is the 2-D action spectrum. The spectrum is plotted versus the normalized wave number in Figure 5 for times ranging from 0 to $2000/\omega_p$. The corresponding results from the models described in this paper are shown in Figures 6 and 7. In this case, the diffusion approximation produces very little energy transfer in the region of the rapid spectral falloff, presumably because of the local nature of this approximation. The modified approximation produces a growth in the high wave number region similar to that seen in *Yokoyama*'s results. We take this as an indication that energy is being transferred over relatively long distances in wave number space. The 1-D action spectrum falls off approximately as k^{-3} in this region, as in *Yokoyama*'s spectrum, and this falloff would continue to higher wave numbers were it not for the artificial dissipation term used in these calculations. The details near the spectral peak and at low wave numbers are slightly different from those in *Yokoyama*'s results, but these differences have not been pursued here because the focus of this paper is on the evolution of the high frequency end of the spectrum.

4. Numerical Solution

[13] For purposes of a stability analysis, (10) can be written in terms of the variable y as

$$\frac{\partial y}{\partial t} = f(y) + D_w \frac{\partial^2 y}{\partial w^2} + D_\phi \frac{\partial^2 y}{\partial \phi^2}, \tag{21}$$

where $D_w = 3\alpha_1 \omega (c_g/c) B^2$ and $D_\phi = 3\alpha_1 \omega (1 - 3\tau k/c_g^2) B^2$. Heuristically, the stability criterion for an explicit numerical solution of (17) is

$$\Delta t \leq \frac{1}{\sqrt{2}\max\left\{ (1/\Delta t_w)^2 + (1/\Delta t_\phi)^2 \right\}^{1/2}}, \text{ where}$$
$$\Delta t_w = \frac{(\Delta w)^2}{2D_w} \text{ and } \Delta t_\phi = \frac{(\Delta \phi)^2}{2D_\phi}, \tag{22}$$

Δw and $\Delta \phi$ being the grid spacings in the logarithmic frequency w and the angle ϕ, respectively [*Press et al.*, 1992]. Note that at high wave numbers the coefficient D_ϕ becomes negative, causing an inherent instability at these wave numbers. To prevent this instability, D_ϕ is set to zero for $3\tau k/c_g^2 > 1$. This procedure probably causes the angular width of the spectrum to be overestimated at high wave numbers but still preserves the main features observed in empirical data (see Figure 10 below).

[14] We have used a second-order Runge-Kutta or midpoint method, with the step size discussed above, to numerically integrate (10). To implement this method, we first evaluate the source function at the current time step and calculate the first-order solution $B_1 = B_0 + F_s(B_0)\Delta t$. We then compute the source function at B_1, take the average of the two source functions $\overline{F}_s = [F_s(B_0) + F_s(B_1)]/2$, and use this to calculate the second-order solution $B_2 = B_0 + \overline{F}_s \Delta t$ at each wave number.

[15] A heuristic stability analysis of (14) can be carried out by writing this equation as

$$\frac{\partial \psi_i}{\partial t} = g(\psi) + \left[D_w \frac{\partial^2 \psi_i}{\partial w^2} + D_\phi \frac{\partial^2 \psi_i}{\partial \phi^2} \right] \Delta w, \tag{23}$$

where $\psi_I = \psi_{i-1} + (w_i/k_i^2) B_i^2 \Delta w$ represents the value of the function defined in (11) at the frequency sample i and $g(\psi)$ is a functional of ψ that includes the derivatives of ψ at other frequency samples but not at the ith sample. The time step size for this formulation is therefore the same as that given in (22) but divided by the logarithmic frequency sample spacing Δw. Equation (14) is then numerically integrated in the same way as previously described, using this modified step size.

[16] In the presence of variable surface currents, i.e., when the advective terms in (3) are included, the evolution

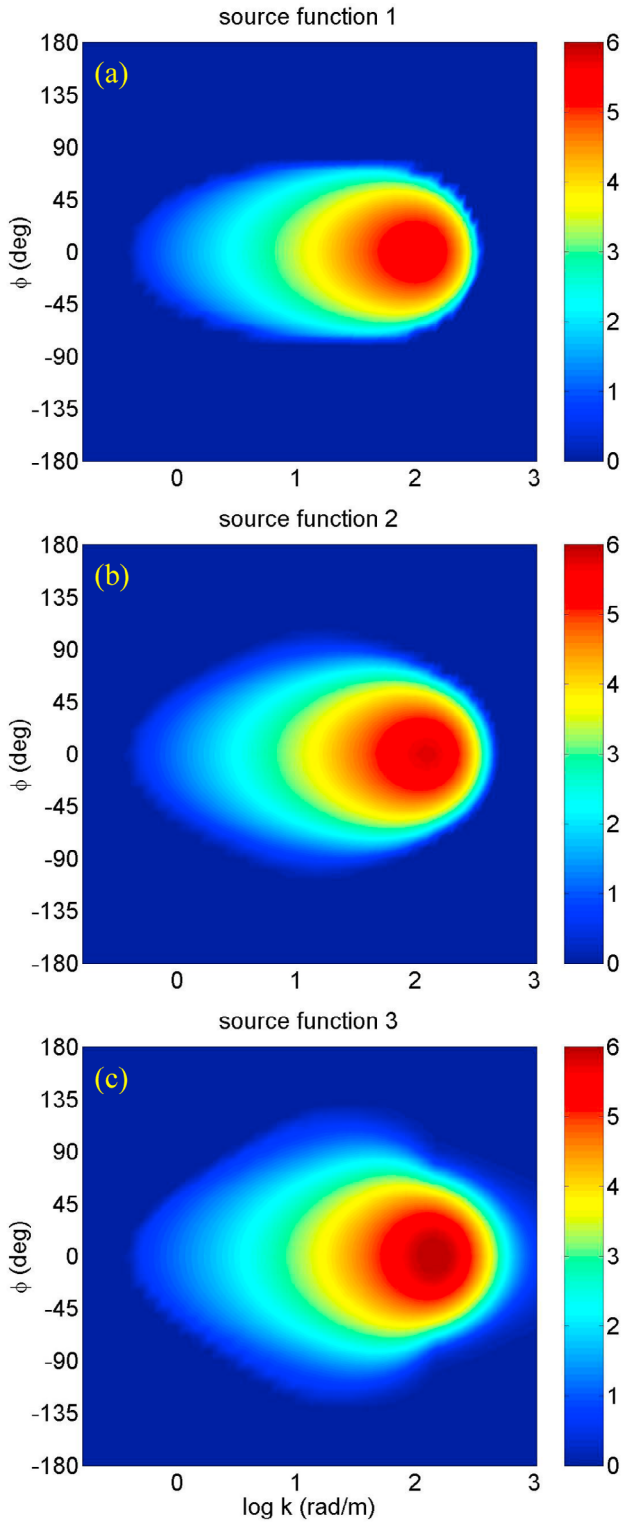

Figure 8. Equilibrium spectra $B(k, \phi)$ for three versions of the net source function, for a wind speed of 5 m/s.

equation for B can be solved using the same method but with a step size given by

$$\Delta t = \frac{1}{\sqrt{5}\max\{|v|\}}, \tag{24}$$

where

$$|v|^2 = (V_x/\Delta x)^2 + (V_w/\Delta w)^2 + (V_\phi/\Delta\phi)^2 + \left(\frac{2D_w}{(\Delta w)^2}\right)^2 + \left(\frac{2D_\phi}{(\Delta\phi)^2}\right)^2 \tag{25}$$

for the original formulation of *Jenkins and Phillips* [2001] and

$$|v|^2 = (V_x/\Delta x)^2 + (V_w/\Delta w)^2 + (V_\phi/\Delta\phi)^2 + \left[\left(\frac{2D_w}{(\Delta w)^2}\right)^2 + \left(\frac{2D_\phi}{(\Delta\phi)^2}\right)^2\right](\Delta w)^2 \tag{26}$$

for the modified formulation using (11) instead of (6). The maximum value is computed over the entire computational grid. A small amount of numerical diffusion in the x direction is also added to damp the spatial oscillations that sometimes occur in the solution, by adding a term $0.01[B(x + \Delta x) - 2B(x) + B(x - \Delta x)]$ to the solution.

[17] The solution of (3) without the nonlinear transfer term can be obtained in the same way by setting $\alpha_1 = 0$, but in this case the step size is given by

$$\Delta t = \frac{1}{\sqrt{3}\max\{|v|\}}, \text{ with}$$
$$|v|^2 = (V_x/\Delta x)^2 + (V_w/\Delta w)^2 + (V_\phi/\Delta\phi)^2. \tag{27}$$

If there are no currents (and the nonlinear transfer term is neglected), the growth equation can be solved analytically using the change of variable $z = 1/(2B^2)$, which results in the equation

$$\frac{\partial z}{\partial t} = \alpha_0\omega - 2\beta' z, \tag{28}$$

where $\beta' = \beta - 4\nu k^2$. This equation has the solution $z = z_0 + z_1 e^{-2\beta' t}$, where $z_0 = \alpha_0\omega/(2\beta')$ and z_1 is determined by the initial value of z. Reversing the change of variable, the solution for B can be written as

$$B(t + \Delta t) = B(t)\left[\frac{\alpha_0\omega}{\beta'}\left(1 - e^{-2\beta'\Delta t}\right)B^2(t) + e^{-2\beta'\Delta t}\right]^{-1/2} \tag{29}$$

for arbitrary Δt. Note that as $\Delta t \to \infty$, this approaches the equilibrium solution

$$B_{\text{in}}(k,\phi) = \begin{cases} \sqrt{(\beta - 4\nu k^2)/(\alpha_0\omega)} & \text{for} \quad \beta > 4\nu k^2 \\ 0 & \text{for} \quad \beta \le 4\nu k^2 \end{cases}. \tag{30}$$

5. Example Results

[18] Results are presented here for three versions of the net source function: (1) a version containing wind input, viscous dissipation, and nonlinear dissipation terms but no energy transfer, (2) the nonlinear energy transfer term of

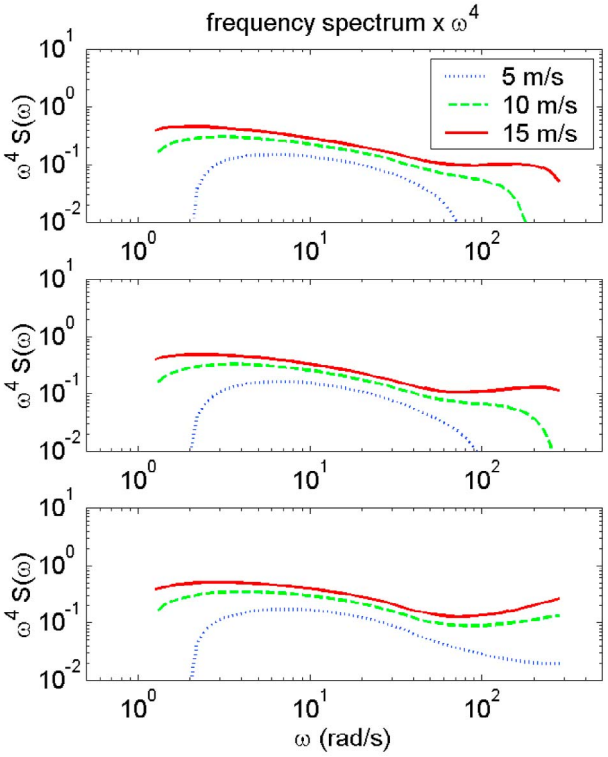

Figure 9. Equilibrium frequency spectra for all three source functions, for wind speeds of 5, 10, and 15 m/s.

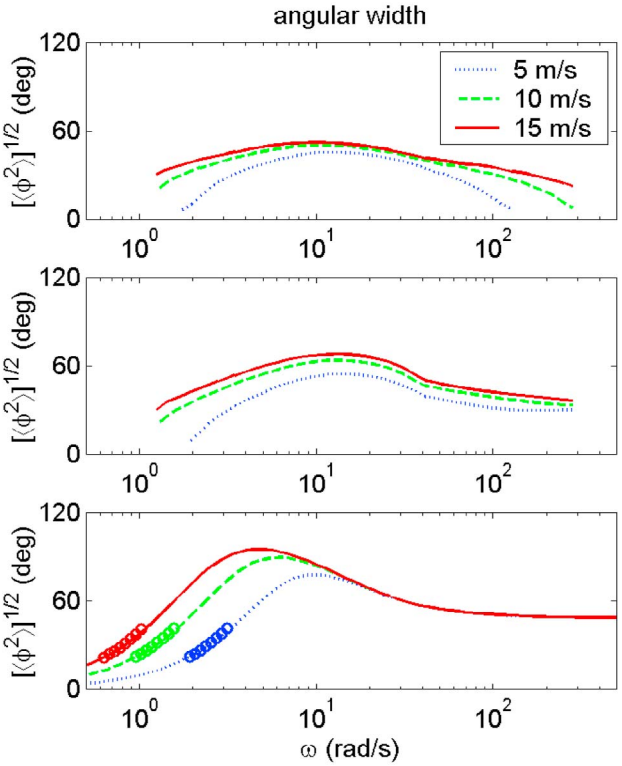

Figure 10. Angular widths of equilibrium spectra for (top) source functions 2 and (center) source function 3 compared with (bottom) model functions of *Donelan et al.* [1985] and *Caudal and Hauser* [1996] (circles and curves, respectively) for three wind speeds.

Jenkins and Phillips [2001], as defined by (5) and (6) with $\alpha_1 = 2.5$, and (3) the modified nonlinear transfer term defined by (5) and (11), with $\alpha_1 = 20$. The wind input term was taken to be that of *Snyder et al.* [1981], as defined by the equation

$$\beta = \beta_o \max[(U_w/c)\cos(\phi > -\phi_w) - 1,\ 0]\,\omega, \qquad (31)$$

where $\beta_o = 3 \times 10^{-3}$, U_w is the wind speed, and ϕ_w is the wind direction. In all three cases, the scale factor for the nonlinear dissipation term was taken as $\alpha_0 = 100$ in order to produce a reasonable magnitude for the equilibrium spectrum. However, no attempt has been made as yet to adjust this parameter or to experiment with other dissipation models in order to optimize the form or magnitude of the equilibrium spectrum.

[19] Plots of the equilibrium spectra for all three cases are shown in Figure 8, for $U_w = 5$ m/s. For version 1 of the source function, the equilibrium spectrum was calculated analytically from (30). For versions 2 and 3, the spectrum was obtained by numerically integrating (10) and (14), respectively, using (30) as the initial value. The time stepping was repeated until the spectrum reached a limiting value, as defined by the criterion $F_s(k, \phi) < 0.005\, B(k, \phi)$ for all (k, ϕ). Note that there is a noticeable increase in the angular spreading, as well as an increase in the spectral density at large wave numbers from cases 1 to 3, but there is a larger difference between 2 and 3 than between 1 and 2.

[20] For comparison with commonly used spectral shapes and measurements, these equilibrium spectra, as well as the corresponding ones for wind speeds of 10 and 15 m/s, were converted into frequency spectra using

$$S(\omega) = \frac{k^{-3}}{c_g}\int_{-\pi}^{\pi} B(k,\phi)\mathrm{d}\phi, \text{ where } \omega^2 = gk + \tau k^3, \qquad (32)$$

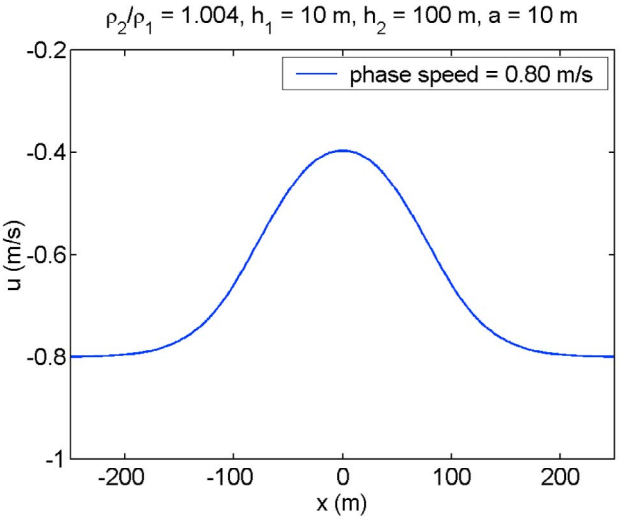

Figure 11. Internal wave surface currents calculated from model of *Choi and Camassa* [1999].

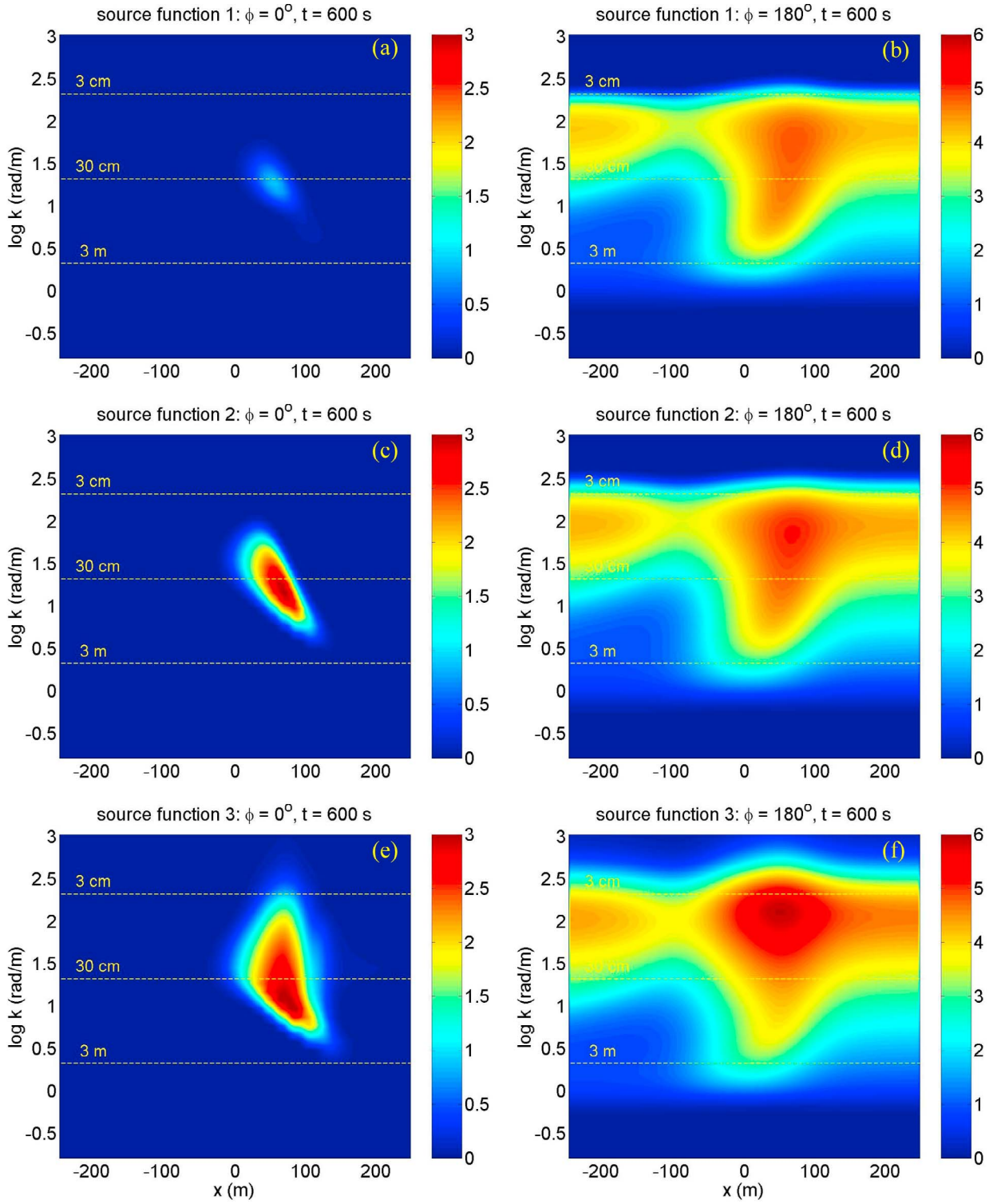

Figure 12. $B(k, \phi, x)$ at (left) $\phi = 0°$ and (right) $\phi = 180°$, for (top) source function 1, (center) source function 2, and (bottom) source function 3.

and the angular width was computed by taking the square root of

$$\langle \phi^2 \rangle = \int_{-\pi}^{\pi} \phi^2 B(k,\phi)\,\mathrm{d}\phi \Big/ \int_{-\pi}^{\pi} B(k,\phi)\,\mathrm{d}\phi. \qquad (33)$$

Figure 9 shows the frequency spectra multiplied by ω^4 for each version of the net source function. No explicit comparisons are made with existing spectral models, because we have not yet attempted to tune the other terms in the net source function, but we note that for source function 3 the quantity

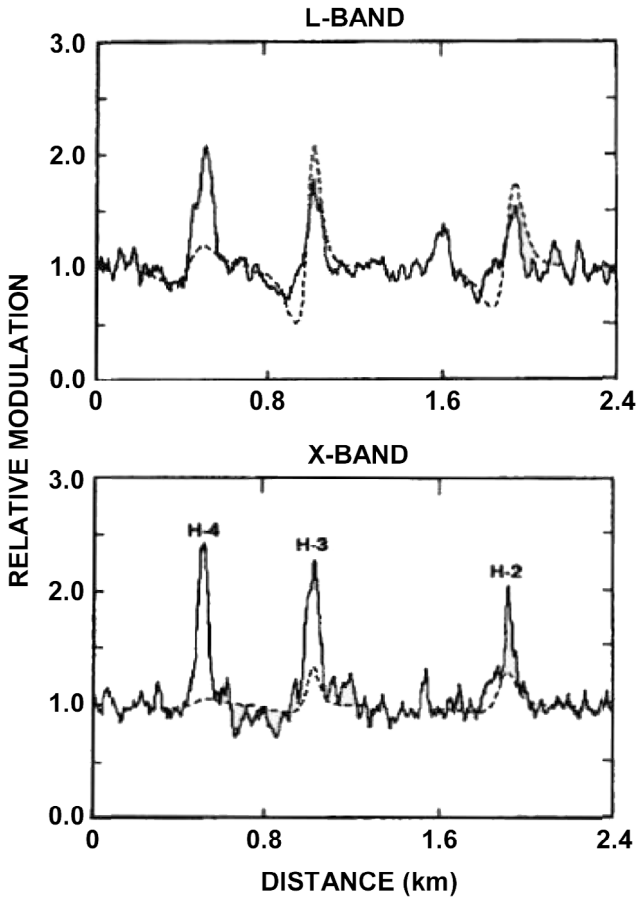

Figure 13. Radar backscatter modulations observed for internal wave packet H during the SAR Internal Wave Experiment [from *Gasparovic et al.*, 1988]. Dashed curves indicate model predictions by *Thompson et al.* [1988].

$\omega^4 S(\omega)$ is nearly flat at intermediate frequencies, in agreement with the measurements of *Donelan et al.* [1985] and consistent with weak turbulence theory [*Zakharov and Pushkarev*, 1999]. The angular widths for source functions 2 and 3 are shown in Figure 10 along with the equivalent angular widths from *Donelan et al.* [1985] and from the *Caudal and Hauser* [1996] spectrum, which is equivalent to the JONSWAP spectrum [*Hasselmann et al.*, 1980] for frequencies below about 4 rad/s but shows a narrowing at higher frequencies as inferred from radar backscatter measurements. Although the quantitative agreement with these model functions is not particularly good, the qualitative changes in spectral width predicted by both versions of the source function are consistent with the model functions shown.

[21] Next, the full wave action equation was integrated using the same three versions of the source function, for a surface current field representative of a moderately strong solitary internal wave. The surface currents were calculated using the model of *Choi and Camassa* [1999] with an upper layer thickness of 10 m, a lower layer thickness of 100 m, a density difference $\Delta\rho/\rho = 0.004$ and a wave amplitude of 10 m. These parameters were chosen to roughly mimic the largest internal waves observed by *Gasparovic et al.* [1988] in the New York Bight. The propagation speed of this internal wave is calculated to be 0.80 m/s, and the surface current in a coordinate system moving with the internal wave is shown in Figure 11 (the propagation direction is to the right in this figure). The wind speed was again chosen to be 5 m/s (as in Figure 8) and the wind direction was chosen to be from 45° relative to the internal wave propagation direction, similar to conditions during the New York Bight experiment. Calculations were done for a time interval of 600 s, starting with the equilibrium spectra shown in Figure 8.

[22] Figure 12 shows the spectral density at $t = 600$ s plotted versus x and k for $\phi = 0°$ (i.e., for waves propagating in the same direction as the internal wave) and for $\phi = 180°$ (waves propagating in the opposite direction). The spectral densities are generally larger at $\phi = 180°$ since this is closer to the wind direction. The peak spectral densities in this direction increase by about 20% from source function 1 to source function 3, and an increase in spectral densities at high wave numbers is apparent in Figure 12 (both center right and bottom right cases), but more dramatically in the latter.

[23] Even more striking differences occur in the spectra at $\phi = 0°$. It may be surprising that any energy at all occurs at this angle, since it is more than 90° from the wind direction. For source function 1 the initial spectral density is nominally zero at this angle, and there is no mechanism for energy to be transferred to this direction. However, an arbitrary initial spectral density of $B_{min} = 1 \times 10^{-10}$ was applied at all wave numbers, in order to allow the wind growth term in (4) to take effect (the source function would remain zero for all time if B were initially zero). Waves having an effective

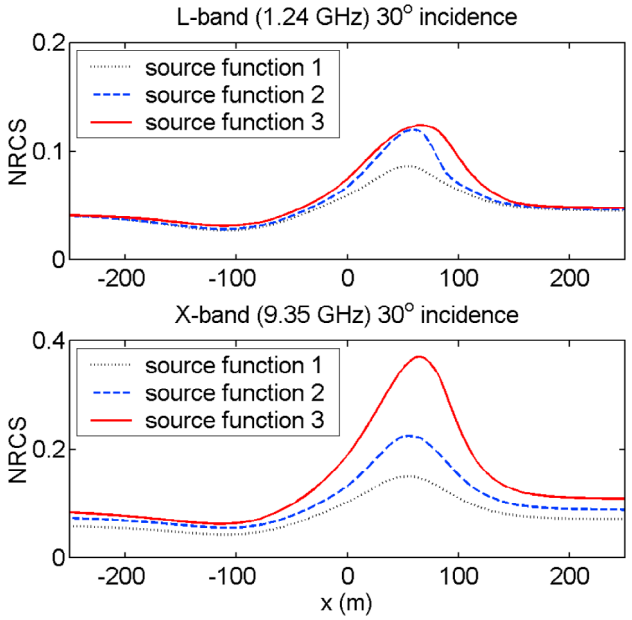

Figure 14. Radar backscatter computed for three versions of the source function, for conditions similar to those in Figure 13.

group velocity ($c_{gx} + u$) equal to the internal wave phase velocity, the so-called "resonant waves," experience a continual input of energy from the internal wave and grow exponentially until limited by dissipation or nonlinear energy transfer. Thus, even very small initial spectral densities at these wave numbers grow and become appreciable or possibly even dominant in some cases. For source functions 2 and 3, energy is transferred into these wave numbers by nonlinear interactions, so this effect occurs regardless of the value of $B_{\min}$ and appears much earlier than for source function 1. Furthermore, the energy pumped into the resonant waves from the internal wave is rapidly transferred to higher wave numbers where it can influence the microwave radar backscatter directly (via increased Bragg scattering) as well as indirectly by surface tilting effects. The spectra at $\phi = 0°$ may in fact continue to grow beyond $t = 600$ s, but the differences are already apparent at this time.

[24] To evaluate the implications of these changes for remote sensing, the radar backscatter was calculated at each grid point using a two-scale scattering model [*Lyzenga*, 2004] along with the spectral perturbations discussed above. Calculations were made for microwave frequencies of 1.24 and 9.35 GHz, and at incidence angles of 30° in order to compare with the L band and X band observations reported by *Gasparovic et al.* [1988] for wave packet H. These observations are shown as the solid curves in Figure 13. Figure 13 also shows a set of predictions by *Thompson et al.* [1988], using a model that did not include nonlinear interactions. This model is similar to that discussed in this paper using source function 1. The calculated radar cross sections using all three source functions are plotted versus position in Figure 14. The differences among the results using these source functions are most pronounced at X band, and the predictions using source function 3 seem to be fairly consistent with the observations in Figure 13. These results appear to resolve a long-standing problem that has been reported in the literature, namely the discrepancy between model predictions and observations at X band, and these results also seem to bear out conjectures by *Gasparovic et al.* [1988] and *Lyzenga and Bennett* [1988], among others, that these underpredictions were due to the neglect of nonlinear hydrodynamic effects in previous models.

6. Conclusions

[25] Nonlinear energy transfer has been incorporated into the wave action equation using the diffusion approximation of *Jenkins and Phillips* [2001] as well as a modified version of their formulation which includes nonlocal spectral effects. The evolution of an initial spectrum due to only this energy transfer is computed and compared with direct numerical simulations by *Tanaka* [2007] and *Yokoyama* [2004]. The wave action equation including traditional wind input and energy dissipation terms as well as the new energy transfer terms is solved as an initial value problem using a second-order Runge-Kutta method, and properties of the solution are examined for one example case. The results illustrate the diffusion of energy in both angle and wave number, and an increase in both the mean spectral density and modulations of the spectral density at high wave numbers. The effects on radar backscatter modulations are calculated using a two-scale scattering model and compared with observations of internal waves in the New York Bight. The results appear to resolve a long-standing discrepancy between model predictions and observations at X band and also seem to bear out conjectures by various authors that these discrepancies were due to the neglect of nonlinear hydrodynamic effects in previous models.

[26] **Acknowledgments.** This work was supported by the National Science Foundation under award DMS-0620750 and by the Office of Naval Research grant N00014-05-1-0273. Wooyoung Choi of the New Jersey Institute of Technology provided a FORTRAN program for calculating internal wave currents and contributed valuable insights at various stages of this research. Helpful comments from two anonymous reviewers were also appreciated and are hereby acknowledged.

References

Caudal, G., and D. Hauser (1996), Directional spreading function of the sea wave spectrum at short scale, inferred from multifrequency radar observations, *J. Geophys. Res.*, *101*, 16,601–16,613, doi:10.1029/96JC00921.

Choi, W., and R. Camassa (1999), Fully nonlinear internal waves in a two-fluid system, *J. Fluid Mech.*, *396*, 1–36.

Donelan, M. A., J. Hamilton, and W. H. Hui (1985), Directional spectra of wind generated waves, *Philos. Trans. R. Soc. London, Ser. A*, *315*, 509–562.

Gasparovic, R. F., J. R. Apel, and E. S. Kasischke (1988), An overview of the SAR internal wave signature experiment, *J. Geophys. Res.*, *93*, 12,304–12,316, doi:10.1029/JC093iC10p12304.

Hasselmann, D. E., M. Dunckel, and J. A. Ewing (1980), Directional wave spectra observed during JONSWAP 1973, *J. Phys. Oceanogr.*, *10*, 1264–1280.

Hasselmann, K. (1962), On the nonlinear energy transfer in a gravity-wave spectrum: Part 1. General theory, *J. Fluid Mech.*, *12*, 481–500.

Jenkins, A. D., and O. M. Phillips (2001), A simple formula for nonlinear wave-wave interaction, *Int. J. Offshore Polar Eng.*, *11*, 81–86.

Lyzenga, D. R. (2004), Ocean wave spectrum and dissipation rate derived from CMOD4 model function, *J. Geophys. Res.*, *109*, C07019, doi:10.1029/2003JC002237.

Lyzenga, D. R., and J. R. Bennett (1988), Full-spectrum modeling of SAR internal wave signatures, *J. Geophys. Res.*, *93*, 12,345–12,354, doi:10.1029/JC093iC10p12345.

Phillips, O. M. (1984), On the response of short ocean wave components at a fixed wave number to ocean current variations, *J. Phys. Oceanogr.*, *14*, 1425–1433.

Phillips, O. M. (1985), Spectral and statistical properties of the equilibrium range in wind-generated gravity waves, *J. Fluid Mech.*, *156*, 505–531.

Plant, W. J. (1982), A relationship between wind stress and wave slope, *J. Geophys. Res.*, *87*, 1961–1967, doi:10.1029/JC087iC03p01961.

Polnikov, V. G. (2002), A basing of the diffusion approximation derivation for the four-wave kinetic integral and properties of the approximation, *Nonlinear Proc. Geophys.*, *9*(3/4), 355–366.

Polnikov, V. G., Y. A. Volkov, and F. A. Pogarskii (2002), Numerical wind wave model with a dynamic boundary layer, *Nonlinear Proc. Geophys.*, *9*(3/4), 367–371.

Press, W. H., S. A. Teukolsky, W. T. Vetterling, and B. P. Flannery (1992), *Numerical Recipes in FORTRAN*, 963 pp., Cambridge Univ. Press, New York, NY.

Resio, D., and W. Perrie (1991), A numerical study of nonlinear energy fluxes due to wave-wave interactions: Part 1. Methodology and basic results, *J. Fluid Mech.*, *223*, 603–629.

Snyder, R. L., F. W. Dobson, J. A. Elliot, and R. B. Long (1981), Array measurements of atmospheric pressure fluctuations above gravity waves, *J. Fluid Mech.*, *102*, 1–59.

Tanaka, M. (2001), Verification of Hasselmans's energy transfer among surface gravity waves by direct numerical simulations of primitive equations, *J. Fluid Mech.*, *444*, 199–221.

Tanaka, M. (2007), On the role of resonant interactions in the short-term evolution of deep-water ocean spectra, *J. Phys. Oceanogr.*, *37*, 1022–1036.

Thompson, D. R. (1988), Calculation of radar backscatter modulations from internal waves, *J. Geophys. Res.*, *93*, 12,371–12,380, doi:10.1029/JC093iC10p12371.

Thompson, D. R., B. L. Gotwols, and R. E. Sterner (1988), A comparison of measured surface wave spectral modulations with predictions from a wave-current interaction model, *J. Geophys. Res.*, *93*, 12,339–12,343, doi:10.1029/JC093iC10p12339.

Yokoyama, N. (2004), Statistics of gravity waves obtained by direct numerical simulation, *J. Fluid Mech.*, *501*, 169–178.

Zakharov, V. E., and A. N. Pushkarev (1999), Diffusion model of interacting gravity waves on the surface of deep fluid, *Nonlinear Proc. Geophys.*, *6*, 1–10.

D. R. Lyzenga, Naval Architecture and Marine Engineering Department, University of Michigan, 2600 Draper Rd., Ann Arbor, MI 48109, USA. (lyzenga@umich.edu)